NANO LETTERS
Letter
Cite This: Nano Lett. 2018, 18, 2943−2949
pubs.acs.org/NanoLett

Surface Vacancy-Induced Switchable Electric Polarization and Enhanced Ferromagnetism in Monolayer Metal Trihalides

Yinghe Zhao, Lingfang Lin, Qionghua Zhou, Yunhai Li, Shijun Yuan, Qian Chen, Shuai Dong,* and Jinlan Wang*

School of Physics, Southeast University, Nanjing 211189, China

Supporting Information

ABSTRACT: Monolayer chromium triiodide (CrI_3), as the thinnest ferromagnetic material demonstrated in experiment [Huang et al. *Nature* **2017**, *546*, 270], opens up new opportunities for the application of two-dimensional (2D) materials in spintronic nanodevices. Atom-thick 2D materials with switchable electric polarization are now urgently needed for their rarity and important roles in nanoelectronics. Herein, we unveil that surface I vacancies not only enhance the intrinsic ferromagnetism of monolayer CrI_3 but also induce switchable electric polarization. I vacancies bring about an out-of-plane polarization without breaking the nonmetallic nature of CrI_3. Meanwhile, the induced polarization can be reversed in a moderate energy barrier, arising from the unique porosity of CrI_3 that contributes to the switch of I vacancies between top and bottom surfaces. Engineering 2D switchable polarization through surface vacancies is also applicable to many other metal trihalides, which opens up a new and general way toward pursuing low-dimensional multifunctional nanodevices.

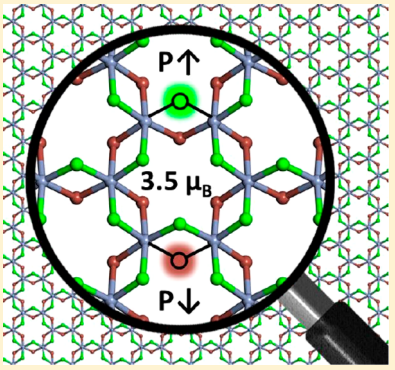

KEYWORDS: *Metal trihalides, monolayer CrI_3, two-dimensional materials, ferromagnetism, switchable electric polarization, out-of-plane polarization*

Since graphite was exfoliated into graphene,[1] atom-thick two-dimensional (2D) materials have emerged as a new frontier and have shown a bright prospect in various fields, such as electronic devices,[2−7] catalysts,[8−12] and energy storage and conversion.[13−18] Compared to those fields, the process has been very slow on the application of 2D materials for spintronics, mainly because of the lack of the magnetic ordering in conventional 2D materials. Therefore, much effort has been devoted to theoretically predicting new 2D ferromagnetic materials by using density functional theory (DFT) calculations,[19−29] among which chromium triiodide (CrI_3) down to monolayer was predicted to be a 2D ferromagnetic material.[23,24] Very recently, a great breakthrough was made by Zhang's group who experimentally demonstrated that 2D ferromagnetic ordering can exist in atom-thick bilayer $Cr_2Ge_2Te_6$.[30] More recently, Xu's group discovered that 2D ferromagnetic ordering really exists in monolayer CrI_3, which is the first experimental evidence on the existence of intrinsic ferromagnetism in atom-thick 2D materials down to monolayer.[31]

In addition to magnetism, electricity is another fundamental concept in physics. Achieving electric polarization in atom-thick 2D materials is also a long-term goal because of the drive toward the miniaturization of electronic devices. Monolayer tin telluride is the first, and so far, only, atom-thick 2D material with switchable electric polarization demonstrated in experiment to the best of our knowledge.[32] However, its electric polarization is in plane rather than out of plane, which limits its practical application severely. It is therefore highly desirable to theoretically search or design new atom-thick 2D materials that are of out-of-plane polarization as potential candidates for experimentalists. The theoretical exploration is very challenging because the qualified materials should meet the following three conditions: (i) atom-thick, (ii) nonmetal, and (iii) out-of-plane polarization. Moreover, it is better that the out-of-plane polarization can be switched to increase the opportunities employed in nanoelectronics. The switchable polarization requires that the qualified materials possess a moderate energy barrier for polarization reversal. As a result, the successful cases are very rare.[33−36]

Magnetism and electricity have a close relationship by relying on the four Maxwell equations, and their combination establishes the unified framework of electromagnetism. If magnetism and electricity appear together in one single 2D material, such a material will certainly bring more possibilities for the design of multifunctional nanodevices. Therefore, it is considerably attractive to explore whether intrinsic ferromagnetism of monolayer CrI_3 can coexist with out-of-plane electric polarization. As is well-known, surface vacancies are inevitable in as-exfoliated and as-synthesized atom-thick 2D materials. Although these vacancies often have a side effect on the charge transport,[37−39] they can enrich the application of 2D materials in other fields.[8,10,11,40−42] Engineering surface vacancy-rich 2D materials and exploring their effect on the properties of 2D

Received: January 22, 2018
Revised: March 23, 2018
Published: April 18, 2018

DOI: 10.1021/acs.nanolett.8b00314
Nano Lett. 2018, 18, 2943−2949

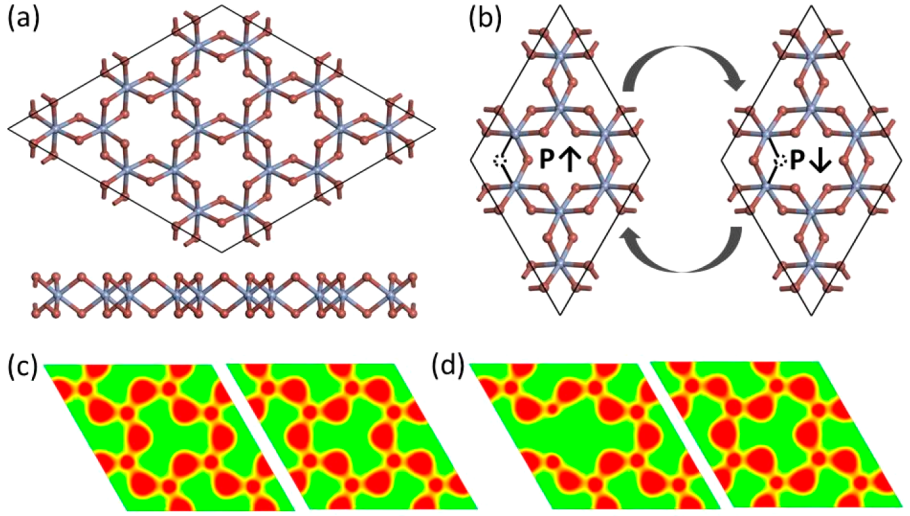

Figure 1. (a) Structure of monolayer CrI_3 from top and side views where I and Cr atoms are represented by red and blue balls. (b) Schematic diagram of IV−CrI_3 working as an atom-thick 2D material with switchable out-of-plane polarization in which the vacancy is represented by the black dotted circle. Charge density distributions of (c) P−CrI_3 and (d) IV−CrI_3 with top I vacancy. The left and the right in parts c and d record the distributions on the top and bottom surfaces, respectively.

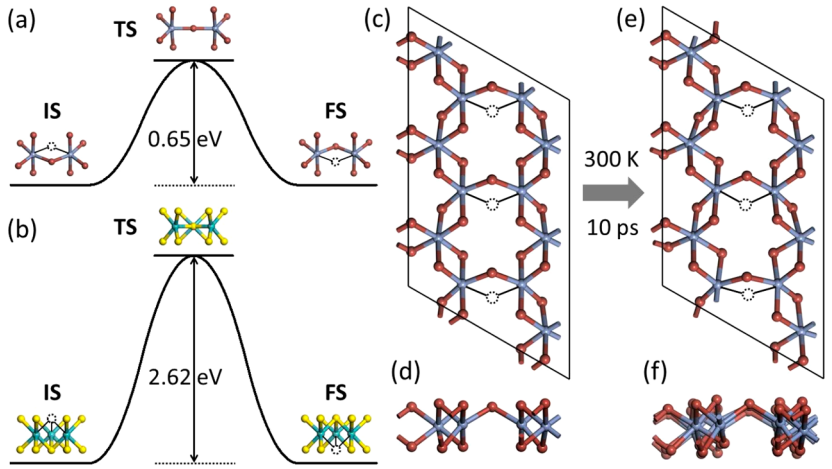

Figure 2. Migration pathways of the (a) I vacancy (the circle) in CrI_3 and (b) S vacancy (the circle) in MoS_2 where yellow and green balls stand for S and Mo atoms. IS, TS, and FS represent the initial state, the transition state, and the final state, respectively. Structure of IV−CrI_3 with vacancy concentration of 1.96×10^{-6} mol/m^2 from (c) top and (d) side views. (e, f) Snapshot of the structure in parts c and d at time of 10 ps during AIMD simulation under the temperature of 300 K.

materials have thus attracted ever-growing attention. In this work, by DFT calculations, we surprisingly discover that surface I vacancies exert positive influences on monolayer CrI_3 from two aspects: (i) inducing switchable out-of-plane polarization and (ii) enhancing intrinsic ferromagnetism. Therefore, monolayer CrI_3 with I vacancies (IV−CrI_3) is an ideal atom-thick 2D material with coexisting intrinsic ferromagnetism and out-of-plane polarization. Furthermore, we demonstrate that achieving 2D switchable polarization through surface vacancies does not just work in CrI_3, and it has a certain degree of generality for other metal trihalides.

The perfect monolayer CrI_3 (P−CrI_3) belongs to the $P\bar{3}1m$ space group (see Figure 1a), whose point group is nonpolar. The charge density distributions of P−CrI_3 on the top and bottom surfaces shown in Figure 1c are of high symmetry, further supporting that the polarization does not exist. To induce the electric polarization, the space-inversion symmetry must be broken in P−CrI_3. It is well-known that surface vacancies are very difficult, if not impossible, to avoid in as-exfoliated or as-synthesized atom-thick 2D materials, and engineering surface vacancy-rich 2D materials is not difficult in experiment with the current technology.[8,37−39] Naturally, it is desirable to explore whether surface I vacancies are able to induce switchable out-of-plane polarization.

With the formation of I vacancies, the symmetry of the charge density distributions on top and bottom surfaces is broken (see Figure 1d), suggesting that there may be an out-of-plane polarization in IV−CrI_3. The standard Berry phase calculation[43] confirms that an out-of-plane polarization indeed exists in IV−CrI_3. Thanks to the symmetry, the energies of two oppositely polarized states—the vacancy on the top and bottom surfaces—are completely identical (see Figure 1b). One I vacancy represents one dipole, and its moment is calculated as follows. The dipole moment is denoted as P↑ with I vacancy on the top surface. When the I vacancy is flipped to the bottom surface, we denote the dipole moment as P↓. As a

DOI: 10.1021/acs.nanolett.8b00314
Nano Lett. 2018, 18, 2943−2949

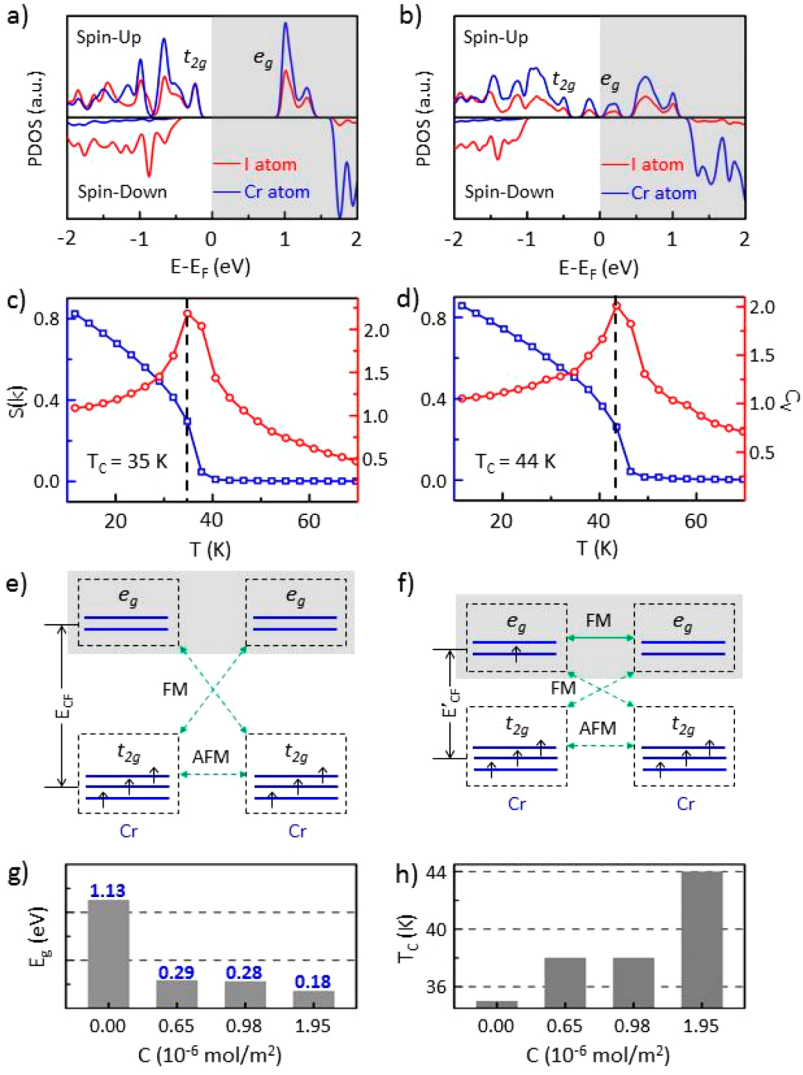

Figure 3. Spin-polarized PDOS of (red line) I and (blue line) Cr of (a) perfect CrI_3, (c) simulated spin structure factor $S(k)$ and specific heat C_V, as well as (e) the corresponding sketch of Cr orbitals and magnetic exchanges of P−CrI_3. Similarly, spin-polarized (b) PDOS, (d) $S(k)$ and C_V, as well as (f) the corresponding sketch of IV−CrI_3 with vacancy concentration of 1.96×10^{-6} mol/m^2 (Figure S2a). E_F, FM, and AFM stand for the Fermi level, ferromagnetic exchange, and antiferromagnetic exchange, respectively. The green solid and dotted lines in parts e and f represent real and virtual hopping, respectively. The crystal field E_{CF} in part e is larger than E'_{CF} in part f. (g) Band gap E_g and (h) Curie temperature T_C of P−CrI_3 and IV−CrI_3 with different vacancy concentrations (Figure S2).

result, the calculated dipole moment of the I vacancy is (P↑ − P↓)/2. The calculated result is 0.13 D which is in the range of experimentally observable dipole moments.[44,45] Interestingly, it is found that the state P↑ or P↓ of one vacancy has negligible effect on the other if not in close proximity. For example, the system energy has negligible change when one of two vacancies in the state P↑ (Figure S1a) is flipped into P↓ (Figure S1b). In other words, there is no coupling among dipoles, and each dipole is isolated. This means that the minimum switchable domain of IV−CrI_3 has the potential to reach one single vacancy, similar to the experimentally proposed single molecule switch.[46−49]

Figure 2a records the process of the polarization reversal of IV−CrI_3 between two oppositely polarized states, i.e., the migration of the I vacancy between the top and bottom surfaces. With the formation of I vacancies, the I atom and its two neighboring Cr atoms constitute a triangle. The calculated transition state is that the I atom just locates between two Cr atoms. Because of the repulsion from the I atom, the distance between two Cr atoms increases to 5.21 Å from 4.47 Å. The calculated energy barrier of 0.65 eV is in the acceptable range, compared with the similar system, e.g., the Sn-atom reversal of SnPc molecule up and down[46] as well as the hydrogen tautomerization of naphthalocyanine molecule,[47,50] showing that the vacancy reversal could be achievable. External stimuli, like mechanical force, electron or hole injection, electric current, electric field, and their combinations that have been successfully used in molecule switches,[46−49,51,52] may be used to trigger the vacancy reversal.

For a comparison with IV−CrI_3, MoS_2 with S vacancies (SV−MoS_2) is also considered, and the transition state of SV−MoS_2 is the S atom just between three neighboring Mo atoms (see Figure 2b). In contrast to that of IV−CrI_3, the calculated energy barrier of SV−MoS_2 is as high as 2.62 eV. Such a difference can be well-explained from the structures of MoS_2 and CrI_3. The close-pack structure of MoS_2 restricts the movement of the atoms neighboring the S vacancy, but the porosity of CrI_3 makes the neighboring atoms to the I vacancy

DOI: 10.1021/acs.nanolett.8b00314
Nano Lett. 2018, 18, 2943−2949

have enough space to relax, thereby enabling the I vacancy to migrate more easily. Therefore, the moderate energy barrier for the polarization reversal of IV−CrI_3 originates from the unique porosity of CrI_3.

The stability of the polarized state at room temperature is of paramount importance for the practical application. In this work, the out-of-plane polarization is contributed by I vacancies; as a result the polarization stability depends on whether I vacancies can resist the thermal disturbance at room temperature. Ab initio molecular dynamics (AIMD) simulation is performed to explore the thermal stability of the IV−CrI_3 structure. Figure 2c,d presents the initial structure of IV−CrI_3 where all I vacancies are at the same side. Under the condition of 300 K, there is no I vacancy migrating to the other side, and they all stay on the same side (see Figure 2e,f). This means that I vacancies have a strong capacity to resist the thermal disturbance, suggesting that the polarized state of IV−CrI_3 can survive stably at room temperature.

The projected density of states (PDOS) of P−CrI_3 is recorded in Figure 3a, whose band gap is 1.13 eV (Figure 3g), in agreement with the previous reports.[23,24] Figure S3 records DOS of IV−CrI_3 with vacancy concentrations of 0.98×10^{-6} and 0.65×10^{-6} mol/m^2, and their band gaps are 0.29 and 0.28 eV (see Figure 3g), respectively. Because of the appearance of defect states around the Fermi level, the band gap of IV−CrI_3 is remarkably narrowed compared to that of P−CrI_3, similar to that of SV−MoS_2.[37,39,53] As shown in Figure 3b,g, the band gap is further reduced to 0.16 eV (0.4 eV at HSE06 calculation level shown in Figure S3d) when the vacancy concentration reaches 1.96×10^{-6} mol/m^2—a very high concentration. That is, the IV−CrI_3 remains a semiconductor, despite its band gap being smaller than that of P−CrI_3.

Next, we explore the effect of I vacancies on the ferromagnetic properties of CrI_3. Prior to the exploration, we compared the calculated magnetic moment of the CrI_3 crystal (3.0 μ_B per Cr atom) with the experimental result (3.1 μ_B per Cr atom).[54] The good agreement between them suggests that our DFT calculation can give an accurate description for the magnetic moment of CrI_3. P−CrI_3 possesses 2D ferromagnetic ordering, and its magnetic moment on each Cr atom is also around 3.0 μ_B. For IV−CrI_3, the symmetry has been broken; consequently, two Cr atoms neighboring the I vacancy (I−Cr atoms) are different from the other Cr atoms. The magnetic moment of the I−Cr atom is increased to 3.5 μ_B, but the others are not influenced by the vacancy. As a result, the total magnetic moment of IV−CrI_3 is increased in comparison with that of P−CrI_3, and it increases with the vacancy concentration. The increased magnetic moment for the I−Cr atom can be understood as follows. Since Cr is in the high spin state, the magnetization equals the number of 3d electrons. Without the vacancy, Cr^{3+} has three 3d electrons, i.e., 3 μ_B. With the vacancy, each I vacancy dopes one electron (i.e., 1 μ_B magnetic moment) to two neighboring I−Cr atoms, thereby leading to the magnetic moment of each I−Cr atom being increased to 3.5 μ_B. As shown in Figures S4 and S5, we construct eight representative magnetic configurations (FM, AF-Neel, AF-zigzag, AF-stripy,[24] etc.) for IV−CrI_3. The calculated energies show that FM is the most stable, which indicates that, like P−CrI_3, IV−CrI_3 prefers 2D ferromagnetic ordering.

We also investigate the influence of I vacancies on the Curie temperature (T_C) of monolayer CrI_3 estimated by using the Metropolis Monte Carlo (MC) simulations.[55] In our MC simulations, the used input includes the exchange interaction J and magnetic anisotropy energy (MAE). MAE is directly obtained by DFT calculation, and J is derived by combining DFT calculation with the Heisenberg spin Hamiltonian. The details on the J calculation and MC simulations can be found in the end of the Supporting Information. The simulated spin structure factor and specific heat for P−CrI_3 are presented in Figure 3c, from which T_C can be determined to be 35 K at the Perdew−Burke−Ernzerhof (PBE) calculation level. At the HSE06 calculation level, the estimated T_C is 46 K, in good agreement with the experimental result 45 K,[31] demonstrating the reliability of our simulation methods. The T_C values of IV−CrI_3 with vacancy concentrations of 0.65, 0.98, and 1.96×10^{-6} mol/m^2 are 38, 38, and 44 K at the PBE level, respectively (see Figure 3d and Figure S6). Importantly, when the concentration is higher, the T_C is higher, as shown in Figure 3h; it is therefore concluded that the I vacancy is able to heighten T_C. The highest T_C that IV−CrI_3 can reach is 52 K (72.5 K at the HSE06 calculation level), about 50% higher than that of P−CrI_3.

The most important contribution for the heightened T_C is the enhanced J between I−Cr atoms. According to the projected DOS (PDOS), as shown in Figure 3a,e, Cr^{3+} possesses the half-filled t_{2g} configuration. According to the Goodenough−Kanamori rule,[56] the exchange between half-filled orbitals is usually antiferromagnetic (see Figure 3e). Thus, for an understanding of the ferromagnetic exchange between Cr−Cr, the empty e_g orbitals must be taken into consideration, which are higher in energy than t_{2g} levels. The virtual hopping between half-filled t_{2g} levels and empty e_g levels leads to the ferromagnetic exchange. With the I vacancy, the e_g levels (and thus reduced crystal field) become closer to the occupied t_{2g} levels (see Figure 3b,f), which can enhance such virtual hopping (and thus ferromagnetic exchange). Furthermore, with partial occupied e_g orbitals, the double-exchange interaction,[57] i.e., real hopping between e_g orbitals, is activated at least around the I vacancy, which is also ferromagnetic. As a result, the effective ferromagnetic exchange is enhanced. The unbroken ferromagnetic ordering, increased magnetic moment, and heightened T_C demonstrate that I vacancies have a positive effect on the ferromagnetism of CrI_3.

For more structural information for experimentalists, we further simulate STM images of IV−CrI_3 with bottom and top I vacancies. Figure 4a depicts the atomic structure of IV−CrI_3 with bottom I vacancies and its corresponding STM image at the bias voltage (V_s) of −2 V. The I atoms on the top surface are much brighter than the Cr atoms and the bottom I atoms. The I vacancy buried in the bottom surface may not be directly observed, but it will lead to the top I atoms opposite to it being brighter than other places. With V_s switched to 1 V, the opposite I atoms are still the brightest, but the top I atoms nearest to the bottom vacancies become dark (see Figure 4b). Top I vacancies can be observed more easily compared to bottom vacancies. As shown in Figure 4c,d, obvious fishlike and round holes appear around top vacancies at V_s = −2 and 1 V, respectively.

Engineering 2D switchable polarization through surface vacancies also applies to other metal trihalides, such as chromium trifluorine (CrF_3), chromium trichlorine ($CrCl_3$), and yttrium trichlorine (YCl_3). Figure 5b records their dipole moment induced by halogen vacancies, that is, 0.24, 0.42, and 0.39 D, respectively. Like IV−CrI_3, CrF_3 and $CrCl_3$ with halogen vacancies are ferromagnetic semiconductors, and the presence of halogen vacancies can increase the magnetic moment of the Cr atoms neighboring them (see Figure 5a).

DOI: 10.1021/acs.nanolett.8b00314
Nano Lett. 2018, 18, 2943−2949

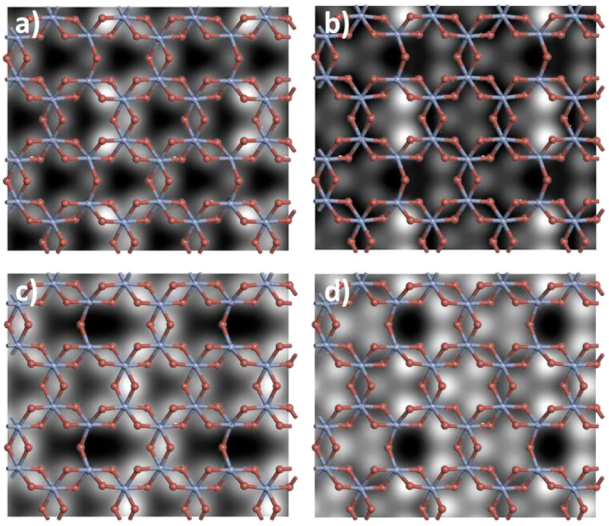

Figure 4. Simulated STM images for IV−CrI_3 with (a, b) bottom I vacancies and (c, d) top I vacancies. (a, c) Images taken at V_s = −2 V and (b, d) images taken at V_s = 1 V. The corresponding atomic structures are placed in the STM images.

Their band gaps are around 0.7 and 1.6 eV, larger than that of IV−CrI_3, but their energy barriers for polarization reversal (0.60 and 0.52 eV) are smaller, as shown in Figure 5c,d. Unlike CrI_3, perfect YCl_3 is a nonmagnetic insulator. The Cl vacancy will narrow the band gap of YCl_3 down to 1.9 eV (Figure 5c), and its migration barrier of ∼0.39 eV (Figure 5d).

In conclusion, we have demonstrated that IV−CrI_3 is an ideal 2D multifunctional material with the coexistence of intrinsic ferromagnetism and switchable out-of-plane polarization by DFT calculations. Such a multifunction originates from four aspects: (i) The structural symmetry of CrI_3 is broken by I vacancies, which induces an out-of-plane polarization. (ii) The porosity of CrI_3 enables I vacancies to migrate between top and bottom surfaces easily, thereby bringing about a moderate energy barrier for the polarization switch. (iii) I vacancies do not break the semiconducting nature of CrI_3. (iv) The ferromagnetic ordering of CrI_3 is not broken by I vacancies, but its ferromagnetism is enhanced. The strategy, utilizing surface vacancies to engineer 2D switchable polarization, is first proposed and generally applicable to many other metal trihalides, such as CrF_3, $CrCl_3$, and YCl_3, with potential applicability to other porous layered materials. Our work expands the opportunities for the application of monolayer CrI_3, establishes an effective strategy to engineer 2D switchable polarization, and discovers a class of desirable 2D materials with switchable out-of-plane polarization, with implications for next-generation nanospintronic and nanoelectronic devices.

Computational Methods. All spin-polarized DFT calculations are implemented in the Vienna ab initio simulation package[58] within a general gradient approximation parametrized by Perdew, Burke, and Ernzerhof (PBE).[59] There are two reasons for choosing the PBE-based DFT calculation: (i) it is the most widely used method in computational materials science, because it achieves a good balance between the computational accuracy and cost; and (ii) it can reproduce the experimental lattice parameters and magnetic moment of the CrI_3 crystal well (see Table S1), suggesting that it should have a high reliability in describing the CrI_3 monolayer. The projected augmented wave method[60] is used to describe the ion−electron interaction, and the kinetic energy cutoff for the plane-wave basis set is set as 500 eV. Three structures with different vacancy concentrations (Figure S2) are constructed, and a vacuum space of greater than 15 Å is introduced. The three structures are relaxed until the forces acting on all atoms are less than 0.01 eV/Å using a *k*-point mesh of 15 × 15 × 1, 9 × 9 × 1, and 7 × 7 × 1, respectively. For an estimation of the exchange interaction and the band gap more accurately, the screened hybrid Heyd−Scuseria−Ernzerhof (HSE06) functional is also used.[61,62] A climbing-image nudged elastic band (cNEB) method[63] is employed to identify the transition states. AIMD simulation is carried out under the canonical ensemble with a time step of 1 fs.

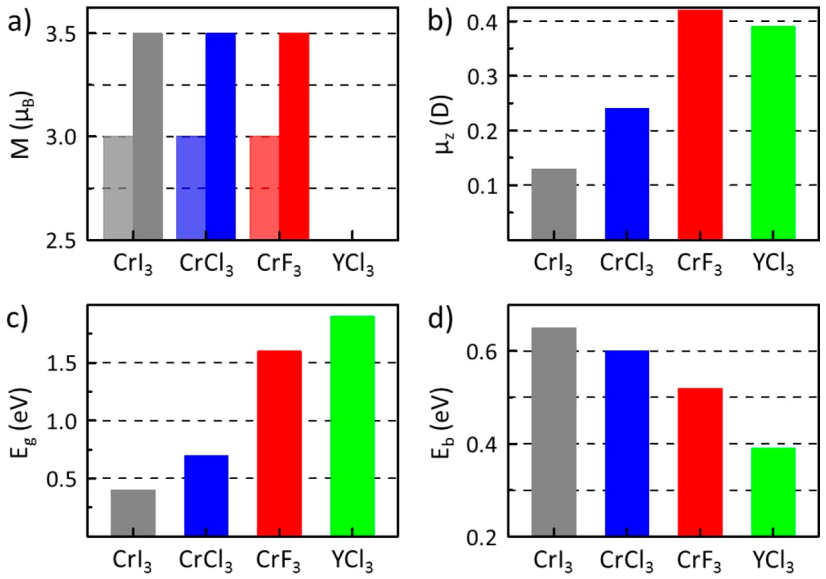

Figure 5. (a) Magnetic moment of two Cr atoms neighboring the vacancy (dark) and the other Cr atoms (light) in CrI_3, $CrCl_3$, and CrF_3 with halogen vacancies. (b) Dipole moment, (c) band gap, and (d) energy barrier for the polarization reversal of CrI_3, $CrCl_3$, CrF_3, and YCl_3 with halogen vacancies. The band gap calculations are based on the HSE06 functional (Figure S7).

DOI: 10.1021/acs.nanolett.8b00314
Nano Lett. 2018, 18, 2943−2949

■ ASSOCIATED CONTENT

Supporting Information

The Supporting Information is available free of charge on the ACS Publications website at DOI: 10.1021/acs.nanolett.8b00314.

Energy difference of P↑ P↑ and P↑ P↓; structures, representative magnetic configurations, DOS, and T_C of monolayer CrI_3; structures and DOS of monolayer $CrCl_3$, CrF_3, and YCl_3; lattice parameters and magnetic moment of the CrI_3 crystal; as well as details on the J calculation and MC simulations (PDF)

■ AUTHOR INFORMATION

Corresponding Authors

*E-mail: jlwang@seu.edu.cn.
*E-mail: sdong@seu.edu.cn.

ORCID

Yinghe Zhao: 0000-0002-2331-8973
Yunhai Li: 0000-0003-4692-8114
Qian Chen: 0000-0002-5793-8185
Shuai Dong: 0000-0002-6910-6319
Jinlan Wang: 0000-0002-4529-874X

Notes

The authors declare no competing financial interest.

■ ACKNOWLEDGMENTS

This work is supported by the National Key Research and Development Program of China (2017YFA0204800), Natural Science Foundation of China (21525311, 21773027, 11674055), Jiangsu 333 project (BRA2016353), the Fundamental Research Funds for the Central Universities of China, and the Scientific Research Foundation of Graduate School of Southeast University (YBJJ1669). The authors are thankful for the computational resources at the SEU and National Supercomputing Centers in Tianjin and Guangzhou.

■ REFERENCES

(1) Novoselov, K. S.; Geim, A. K.; Morozov, S. V.; Jiang, D.; Zhang, Y.; Dubonos, S. V.; Grigorieva, I. V.; Firsov, A. A. *Science* **2004**, *306*, 666−669.
(2) Radisavljevic, B.; Radenovic, A.; Brivio, J.; Giacometti, V.; Kis, A. *Nat. Nanotechnol.* **2011**, *6*, 147−150.
(3) Li, H.; Wu, J.; Yin, Z.; Zhang, H. *Acc. Chem. Res.* **2014**, *47*, 1067−1075.
(4) Li, L.; Yu, Y.; Ye, G. J.; Ge, Q.; Ou, X.; Wu, H.; Feng, D.; Chen, X. H.; Zhang, Y. *Nat. Nanotechnol.* **2014**, *9*, 372−377.
(5) Miró, P.; Audiffred, M.; Heine, T. *Chem. Soc. Rev.* **2014**, *43*, 6537−6554.
(6) Tao, L.; Cinquanta, E.; Chiappe, D.; Grazianetti, C.; Fanciulli, M.; Dubey, M.; Molle, A.; Akinwande, D. *Nat. Nanotechnol.* **2015**, *10*, 227−231.
(7) Ghorbani-Asl, M.; Kuc, A.; Miró, P.; Heine, T. *Adv. Mater.* **2016**, *28*, 853−856.
(8) Li, H.; Tsai, C.; Koh, A. L.; Cai, L.; Contryman, A. W.; Fragapane, A. H.; Zhao, J.; Han, H. S.; Manoharan, H. C.; Abild-Pedersen, F.; Norskov, J. K.; Zheng, X. *Nat. Mater.* **2016**, *15*, 48−53.
(9) Deng, D.; Novoselov, K. S.; Fu, Q.; Zheng, N.; Tian, Z.; Bao, X. *Nat. Nanotechnol.* **2016**, *11*, 218−230.
(10) Zhao, J.; Chen, Z. *J. Am. Chem. Soc.* **2017**, *139*, 12480−12487.
(11) Liu, G.; Robertson, A. W.; Li, M. M.-J.; Kuo, W. C. H.; Darby, M. T.; Muhieddine, M. H.; Lin, Y.-C.; Suenaga, K.; Stamatakis, M.; Warner, J. H.; Tsang, S. C. E. *Nat. Chem.* **2017**, *9*, 810−816.
(12) Liu, Y.; Wu, J.; Hackenberg, K. P.; Zhang, J.; Wang, Y. M.; Yang, Y.; Keyshar, K.; Gu, J.; Ogitsu, T.; Vajtai, R.; Lou, J.; Ajayan, P. M.; Wood, B. C.; Yakobson, B. I. *Nat. Energy* **2017**, *2*, 17127.
(13) Lukatskaya, M. R.; Mashtalir, O.; Ren, C. E.; Dall'Agnese, Y.; Rozier, P.; Taberna, P. L.; Naguib, M.; Simon, P.; Barsoum, M. W.; Gogotsi, Y. *Science* **2013**, *341*, 1502−1505.
(14) Jing, Y.; Zhou, Z.; Cabrera, C. R.; Chen, Z. *J. Mater. Chem. A* **2014**, *2*, 12104−12122.
(15) Dai, J.; Zeng, X. C. *J. Phys. Chem. Lett.* **2014**, *5*, 1289−1293.
(16) Bonaccorso, F.; Colombo, L.; Yu, G.; Stoller, M.; Tozzini, V.; Ferrari, A. C.; Ruoff, R. S.; Pellegrini, V. *Science* **2015**, *347*, 1246501−1246501.
(17) Ma, L.; Dai, J.; Zeng, X. C. *Adv. Energy Mater.* **2017**, *7*, 1601731.
(18) Tan, C.; Cao, X.; Wu, X.-J.; He, Q.; Yang, J.; Zhang, X.; Chen, J.; Zhao, W.; Han, S.; Nam, G.-H.; Sindoro, M.; Zhang, H. *Chem. Rev.* **2017**, *117*, 6225−6331.
(19) Zhou, J.; Sun, Q. *J. Am. Chem. Soc.* **2011**, *133*, 15113−15119.
(20) Ma, Y.; Dai, Y.; Guo, M.; Niu, C.; Zhu, Y.; Huang, B. *ACS Nano* **2012**, *6*, 1695−1701.
(21) Kan, M.; Zhou, J.; Sun, Q.; Kawazoe, Y.; Jena, P. *J. Phys. Chem. Lett.* **2013**, *4*, 3382−3386.
(22) Lebègue, S.; Björkman, T.; Klintenberg, M.; Nieminen, R. M.; Eriksson, O. *Phys. Rev. X* **2013**, *3*, 031002.
(23) McGuire, M. A.; Dixit, H.; Cooper, V. R.; Sales, B. C. *Chem. Mater.* **2015**, *27*, 612−620.
(24) Zhang, W.-B.; Qu, Q.; Zhu, P.; Lam, C.-H. *J. Mater. Chem. C* **2015**, *3*, 12457−12468.
(25) Wu, F.; Huang, C.; Wu, H.; Lee, C.; Deng, K.; Kan, E.; Jena, P. *Nano Lett.* **2015**, *15*, 8277−8281.
(26) Wang, Y.; Wang, S.-S.; Lu, Y.; Jiang, J.; Yang, S. A. *Nano Lett.* **2016**, *16*, 4576−4582.
(27) Kumar, H.; Frey, N. C.; Dong, L.; Anasori, B.; Gogotsi, Y.; Shenoy, V. B. *ACS Nano* **2017**, *11*, 7648−7655.
(28) Dong, L.; Kumar, H.; Anasori, B.; Gogotsi, Y.; Shenoy, V. B. *J. Phys. Chem. Lett.* **2017**, *8*, 422−428.
(29) Sun, Y.; Zhuo, Z.; Wu, X.; Yang, J. *Nano Lett.* **2017**, *17*, 2771−2777.
(30) Gong, C.; Li, L.; Li, Z.; Ji, H.; Stern, A.; Xia, Y.; Cao, T.; Bao, W.; Wang, C.; Wang, Y.; Qiu, Z.; Cava, R.; Louie, S. G.; Xia, J.; Zhang, X. *Nature* **2017**, *546*, 265−269.
(31) Huang, B.; Clark, G.; Navarro-Moratalla, E.; Klein, D. R.; Cheng, R.; Seyler, K. L.; Zhong, D.; Schmidgall, E.; McGuire, M. A.; Cobden, D. H.; Yao, W.; Xiao, D.; Jarillo-Herrero, P.; Xu, X. *Nature* **2017**, *546*, 270−273.
(32) Chang, K.; Liu, J.; Lin, H.; Wang, N.; Zhao, K.; Zhang, A.; Jin, F.; Zhong, Y.; Hu, X.; Duan, W.; Zhang, Q.; Fu, L.; Xue, Q.-K.; Chen, X.; Ji, S.-H. *Science* **2016**, *353*, 274−278.
(33) Shirodkar, S. N.; Waghmare, U. V. *Phys. Rev. Lett.* **2014**, *112*, 157601.
(34) Ding, W.; Zhu, J.; Wang, Z.; Gao, Y.; Xiao, D.; Gu, Y.; Zhang, Z.; Zhu, W. *Nat. Commun.* **2017**, *8*, 14956.
(35) Chandrasekaran, A.; Mishra, A.; Singh, A. K. *Nano Lett.* **2017**, *17*, 3290−3296.
(36) Yang, Q.; Xiong, W.; Zhu, L.; Gao, G.; Wu, M. *J. Am. Chem. Soc.* **2017**, *139*, 11506−11512.
(37) Qiu, H.; Xu, T.; Wang, Z.; Ren, W.; Nan, H.; Ni, Z.; Chen, Q.; Yuan, S.; Miao, F.; Song, F.; Long, G.; Shi, Y.; Sun, L.; Wang, J.; Wang, X. *Nat. Commun.* **2013**, *4*, 2642.
(38) Yu, Z.; Pan, Y.; Shen, Y.; Wang, Z.; Ong, Z.-Y.; Xu, T.; Xin, R.; Pan, L.; Wang, B.; Sun, L.; Wang, J.; Zhang, G.; Zhang, Y. W.; Shi, Y.; Wang, X. *Nat. Commun.* **2014**, *5*, 5290.
(39) Bertolazzi, S.; Bonacchi, S.; Nan, G.; Pershin, A.; Beljonne, D.; Samorì, P. *Adv. Mater.* **2017**, *29*, 1606760.
(40) Kim, J.-S.; Yoo, H.-W.; Choi, H. O.; Jung, H.-T. *Nano Lett.* **2014**, *14*, 5941−5947.
(41) Li, Q.; Zhao, Y.; Ling, C.; Yuan, S.; Chen, Q.; Wang, J. *Angew. Chem., Int. Ed.* **2017**, *56*, 10501−10505.
(42) Nguyen, L.; Komsa, H.-P.; Khestanova, E.; Kashtiban, R. J.; Peters, J. J. P.; Lawlor, S.; Sanchez, A. M.; Sloan, J.; Gorbachev, R. V.;

DOI: 10.1021/acs.nanolett.8b00314
Nano Lett. 2018, 18, 2943−2949

Grigorieva, I. V.; Krasheninnikov, A. V.; Haigh, S. J. *ACS Nano* **2017**, *11*, 2894−2904.
(43) King-Smith, R. D.; Vanderbilt, D. *Phys. Rev. B: Condens. Matter Mater. Phys.* **1993**, *47*, 1651−1654.
(44) Seki, S.; Yu, X. Z.; Ishiwata, S.; Tokura, Y. *Science* **2012**, *336*, 198−201.
(45) Lee, M.; Choi, E. S.; Huang, X.; Ma, J.; Dela Cruz, C. R.; Matsuda, M.; Tian, W.; Dun, Z. L.; Dong, S.; Zhou, H. D. *Phys. Rev. B: Condens. Matter Mater. Phys.* **2014**, *90*, 224402.
(46) Wang, Y.; Kröger, J.; Berndt, R.; Hofer, W. A. *J. Am. Chem. Soc.* **2009**, *131*, 3639−3643.
(47) Liljeroth, P.; Repp, J.; Meyer, G. *Science* **2007**, *317*, 1203−1206.
(48) Zhang, J. L.; Xu, J. L.; Niu, T. C.; Lu, Y. H.; Liu, L.; Chen, W. *J. Phys. Chem. C* **2014**, *118*, 1712−1718.
(49) Zhang, J. L.; Zhong, J. Q.; Lin, J. D.; Hu, W. P.; Wu, K.; Xu, G. Q.; Wee, A. T. S.; Chen, W. *Chem. Soc. Rev.* **2015**, *44*, 2998−3022.
(50) Sarhan, A.; Arboleda, N. B., Jr; David, M.; Nakanishi, H.; Kasai, H. *J. Phys.: Condens. Matter* **2009**, *21*, 064201.
(51) Moresco, F.; Meyer, G.; Rieder, K.-H. *Phys. Rev. Lett.* **2001**, *86*, 672−675.
(52) Choi, B.-Y.; Kahng, S.-J.; Kim, S.; Kim, H.; Kim, H. W.; Song, Y. J.; Ihm, J.; Kuk, Y. *Phys. Rev. Lett.* **2006**, *96*, 156106.
(53) Krivosheeva, A. V.; Shaposhnikov, V. L.; Borisenko, V. E.; Lazzari, J.-L.; Waileong, C.; Gusakova, J.; Tay, B. K. *J. Semicond.* **2015**, *36*, 122002.
(54) Dillon, J. F.; Olson, C. E. *J. Appl. Phys.* **1965**, *36*, 1259−1260.
(55) Dong, S.; Yu, R.; Yunoki, S.; Liu, J.-M.; Dagotto, E. *Phys. Rev. B: Condens. Matter Mater. Phys.* **2008**, *78*, 064414.
(56) Goodenough, J. B. *Scholarpedia* **2008**, *3*, 7382.
(57) Zener, C. *Phys. Rev.* **1951**, *82*, 403−405.
(58) Kresse, G.; Furthmüller, J. *Phys. Rev. B: Condens. Matter Mater. Phys.* **1996**, *54*, 11169−11186.
(59) Perdew, J. P.; Burke, K.; Ernzerhof, M. *Phys. Rev. Lett.* **1996**, *77*, 3865−3868.
(60) Blöchl, P. E. *Phys. Rev. B: Condens. Matter Mater. Phys.* **1994**, *50*, 17953−17979.
(61) Heyd, J.; Scuseria, G. E.; Ernzerhof, M. *J. Chem. Phys.* **2003**, *118*, 8207−8215.
(62) Heyd, J.; Scuseria, G. E.; Ernzerhof, M. *J. Chem. Phys.* **2006**, *124*, 219906.
(63) Henkelman, G.; Uberuaga, B. P.; Jónsson, H. *J. Chem. Phys.* **2000**, *113*, 9901−9904.

DOI: 10.1021/acs.nanolett.8b00314
Nano Lett. 2018, 18, 2943−2949